Proc. Lunar Sci. Conf. 8th (1977), p. 793–811.
Printed in the United States of America

Solar cosmic ray produced noble gases and tracks in lunar fines 10084 and 14163

K. GOPALAN, J. N. GOSWAMI, M. N. RAO, K. M. SUTHAR, and T. R. VENKATESAN

Physical Research Laboratory, Navrangpura, Ahmedabad 380009, India

Abstract—Lunar fines 10084 and 14163 (40–90 and 90–200 μ size fractions) were etched in a controlled manner to remove the surface-correlated solar wind so that the less-abundant components due to solar and galactic cosmic ray spallation could be clearly distinguished. The etched samples were analysed mass-spectrometrically for isotopic abundances of Ne, Ar, and Xe in incremental temperature steps whereas the track density measurements on unetched samples were carried out by both optical and scanning electron microscopy. The neon results indicate the presence of a solar flare proton-produced neon component with a 21/22 ratio of about 0.5. Analysis of xenon data shows significant ^{132}Xe excesses due to SCR contribution after applying usual corrections due to GCR and fission contribution. Similar excesses are also seen for ^{129}Xe and ^{131}Xe. The spallation spectra for the solar flare proton-produced xenon, deduced in the present work are consistent with those obtained from the laboratory experiments of low-energy (38 and 50 MeV) proton-induced spallation reactions in Ba. Using appropriate production rates, "solar flare" exposure ages of 10084 and 14163 are calculated to be about 50 and 100 m.y., which are in satisfactory agreement with the fossil track based "surface" exposure ages of these samples.

INTRODUCTION

LUNAR SURFACE SAMPLES are subjected to galactic and solar cosmic ray (GCR and SCR) bombardment over long periods of time. GCR-produced stable- and radionuclides and particle tracks have been extensively studied in lunar rocks and fines in the past decade. The SCR-effects which are restricted to the first few millimeters of lunar surface have been pursued in detail using solar flare tracks, thermoluminescence and radionuclides such as ^{26}Al and ^{53}Mn, to understand the behaviour of ancient solar cosmic rays (Arrhenius *et al.*, 1971; Hoyt *et al.*, 1973; Shedlovsky *et al.*, 1970). However, in noble gas studies the SCR-effects received limited attention presumably because the large abundance of solar wind noble gases in lunar fines mask the relatively small abundance of SCR-produced noble gas isotopes.

Solar and galactic cosmic rays induce spallation reactions in lunar regolith samples leading to compositionally distinct spallation spectra for noble gases. Walton *et al.* (1974) and Frick *et al.* (1975) showed marginal evidence for SCR-produced Ne in lunar fines 67701 and in 15421 feldspars. Attempts made by Leich *et al.* (1975) to observe the directly-implanted solar flare neon in lunar ilmenites yielded negative results. Previously Rao *et al.* (1971) and Gopalan and Rao (1975) pointed out that solar cosmic ray protons induce low-energy nuclear reactions in Ba of lunar fines and the resulting ^{132}Xe excesses correlate positively with SCR-produced fossil tracks in certain soil samples.

In this paper, we present evidence for the presence of solar flare produced noble gas component in lunar soils with the help of combined mass-spectrometric and fossil track measurements. A selective etching procedure is employed to remove the major portion of surface-correlated solar wind noble gases from these samples and the etched grain size fractions are analysed mass spectrometrically by stepwise heating techniques to further resolve the volume-correlated SCR and GCR spallation and fission components. Fossil track analyses were carried out to determine the solar flare irradiation records in the analysed soils.

EXPERIMENTAL PROCEDURES

Bulk soils 10084 and 14163 were separated into 40–90 and 90–200 μ size fractions by dry-sieving using fresh nylon sieves. In addition we obtained 200–1000 μ size fraction for 10084 only. The 40–90, 90–200 and 200–1000 μ size fractions are labelled A, B, and C, respectively in the following text. These size fractions were etched for a few seconds using a mixture of ultrapure HF and $HClO_4$. After etching, the supernate was analysed for Fe, Mg, Al, Ca, and Na by atomic absorption spectrophotometry. About a micron of the surface layer is estimated to have been etched away in each size fraction assuming that the elemental contents in the solution are mainly from plagioclase and pyroxene. This method of estimation is similar to the one described by Eberhardt *et al.* (1965) for Khor Temiki.

Fossil track studies

For fossil track analysis individual feldspar and pyroxene crystals were hand-picked from the unetched A and B size fractions of the soil samples. Separate grain mounts were made for each size fractions following the procedures described by Bhandari *et al.* (1972). The grains were etched for revelation of tracks using standard recipes (Lal *et al.*, 1968). Track density measurements in the B fractions were carried out using an optical microscope, while scanning electron microscope was used to observe tracks in the A fractions.

Mass spectrometry

The etched samples were wrapped in ultrapure aluminium foils and out-gassed at 150°C for two days. Samples were subjected to stepwise heating analysis in a molybdenum crucible using R.F. induction heating. Noble gases were extracted in a series of 1 hr heatings. After purification procedure (Gopalan and Rao, 1976; Agrawal *et al.*, 1974) Ne and Ar were selectively desorbed from activated charcoal at liquid nitrogen and dry-ice temperatures whereas Xe was desorbed at 110°C. All gases were measured in a Reynolds-type glass mass spectrometer operated with a source magnet and an electron multiplier collecter (Gopalan and Rao, 1976; Gopalan *et al.*, 1973). Nine air spikes, delivered from a metal gas pipette were run during this investigation to check for consistency in mass discrimination and sensitivity calibrations. The spectrometer sensitivities for different noble gases are ^{22}Ne: 1.3×10^{-10}; ^{36}Ar: 0.97×10^{-10}; and ^{132}Xe: 1.4×10^{-13} (all in units of cc STP/mv). In the step-wise heating runs, the temperature of each step was measured with an optical pyrometer and is accurate to within ± 50°C. All data presented in this paper are corrected for blanks at each individual temperature using atmospheric compositions. The blank measurements are usually carried out at the beginning and end of each set of temperature sequences and the average values are given below the tables. The reproducibility of blanks is about 10%. The experimental data are corrected for mass discrimination and it is about 1.5%, 1.2%, and 0.9% for Ne, Ar, and Xe respectively. The uncertainty in the gas contents is about 10% for neon and argon and about 15% for xenon.

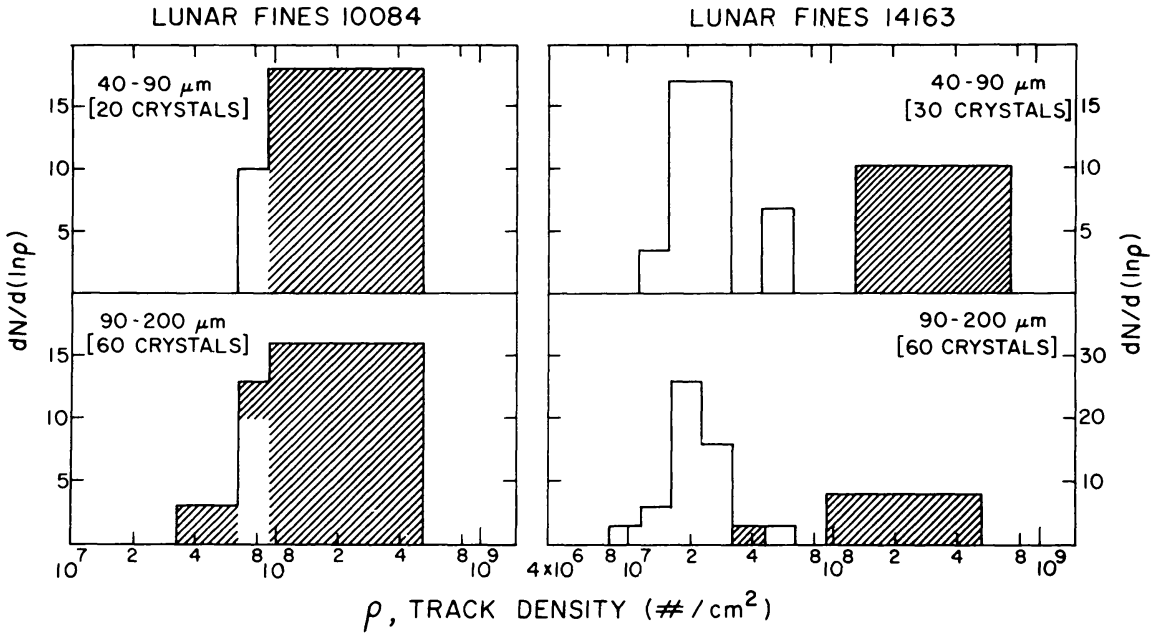

Fig. 1. Track density frequency distributions for the two size fractions of lunar fines 10084 and 14163. The number of crystals has been normalised to 100 in each case. Solar flare irradiated crystals are indicated by the shaded region.

Results and Data Analysis

Fossil tracks

We show in Fig. 1 the results of the track density frequency distribution in the two size fractions for both the soil samples. The crystals that have received detectable solar flare irradiation, as identified from the presence of a track gradient and/or high track densities ($\geqslant 10^8\,cm^{-2}$), are indicated by the shaded region. It can be easily seen that 10084 has received a higher solar flare irradiation dose compared to 14163.

Mass Spectrometry

The elemental and isotopic abundances of neon, argon, and xenon measured in different etched size fractions of soils 14163 and 10084 are given in Tables 1–4. The neon and xenon isotopic ratios from these tables are plotted in several three isotope correlation diagrams (Figs. 2–8). The procedures used for graphical representation are briefly outlined below.

Isotope correlation diagrams

In a two component system, data points representing various mixtures of the end members fall on a line joining the two end members. The points deviating from this "mixing" line are suggestive of the presence of more than two components in the system. The choice of the compositions of the two end

Table 1. Concentration and isotopic composition of neon and argon in two size fractions of 14163 soil.

Size fraction*	Temperature fraction	^{22}Ne (10^{-8}cc STP/g)	^{36}Ar (10^{-8}cc STP/g)	$^{20}Ne/^{22}Ne$	$^{21}Ne/^{22}Ne$	$^{38}Ar/^{36}Ar$	$^{40}Ar/^{36}Ar$
A	550°C	136.0 ± 14.0	398.0 ± 40.0	12.57 ± 0.13	0.0496 ± 0.0010	0.2114 ± 0.0020	28.70 ± 0.29
		194.0 ± 20.0	129.0 ± 13.0	11.27 ± 0.11	0.0704 ± 0.0014	0.2569 ± 0.0026	30.06 ± 0.31
	1250°C	116.0 ± 12.0	96.0 ± 9.6	8.31 ± 0.09	0.2403 ± 0.0048	0.3766 ± 0.0040	36.78 ± 0.38
	1550°C	22.8 ± 2.3	16.0 ± 1.6	10.54 ± 0.11	0.0417 ± 0.0008	0.2215 ± 0.0025	228.1 ± 2.4
	Total	468.0 ± 47.0	638.0 ± 64.0	10.88 ± 0.11	0.1049 ± 0.0021	0.2456 ± 0.0026	35.17 ± 0.35
B	550°C	275.0 ± 27.0	584.0 ± 58.0	12.17 ± 0.12	0.0622 ± 0.0012	0.2039 ± 0.0021	8.09 ± 0.08
	950°C	692.0 ± 69.0	1723.0 ± 172.0	11.88 ± 0.12	0.0586 ± 0.0012	0.2177 ± 0.0022	5.45 ± 0.05
	1250°C	236.0 ± 23.0	1785.0 ± 178.0	10.18 ± 0.10	0.1431 ± 0.0029	0.2154 ± 0.0026	5.11 ± 0.05
	1550°C	5.06 ± 0.50	145.0 ± 14.5	8.14 ± 0.08	0.0841 ± 0.0017	0.2344 ± 0.0024	9.91 ± 0.10
	Total	1208.0 ± 121.0	4237.0 ± 424.0	11.59 ± 0.12	0.0760 ± 0.0015	0.2154 ± 0.0022	5.82 ± 0.06
	Blanks	($\times 10^{-8}$ cc STP) ^{22}Ne: 0.008 (550°C); 0.01 (950°C); 0.05 (1250°C); 0.142 (1550°C); ^{36}Ar: 0.04 (550°C); 0.05 (950°C); 0.048 (1250°C); 0.116 (1550°C)					

*A = 40–90 μ; B = 90–200 μ.

The radiogenic ^{40}Ar in the 40–90 and 90–200 μ size fractions is 2.25×10^{-4} and 2.46×10^{-4} cc STP/g respectively. For a K-content of 0.48% in 14163 (Bogard and Nyquist, 1972) the average value of ^{40}Ar yields a K–Ar age of 3.8 b.y.

members, trapped and spallation components, is made as follows. The BEOC-12 composition (Eberhardt *et al.*, 1972) is assumed to be representative of the trapped component. For the spallation end-point, we have used xenon isotopic composition measured in lunar rocks from the same site as the soil under study. The GCR spallation for 14163 is the average value of Apollo 14 rocks (Marti *et al.*, 1973). For 10084, it is the average value for Apollo 11 rocks (Marti *et al.*, 1970; Eberhardt *et al.*, 1974).

Table 2. Isotopic abundances of xenon in two size fractions of etched 14163 soil.

Size fraction*	Temperature fraction	(^{132}Xe) (10^{-10}cc STP/g)	124	126	128	129	130	131	134	136
A	550°C	13.4 ± 2.0	0.0084 ± 0.0002	0.0124 ± 0.0002	0.0872 ± 0.0013	0.9714 ± 0.0097	0.1428 ± 0.0021	0.8300 ± 0.0083	0.3726 ± 0.0037	0.3150 ± 0.0031
	950°C	6.07 ± 0.91	0.0323 ± 0.0006	0.0451 ± 0.0009	0.1445 ± 0.0022	1.0570 ± 0.0110	0.1905 ± 0.0030	1.2570 ± 0.0130	0.3578 ± 0.0037	0.2857 ± 0.0029
	1250°C	5.3 ± 0.80	0.0847 ± 0.0017	0.1470 ± 0.0029	0.3457 ± 0.0052	1.1430 ± 0.0114	0.3099 ± 0.0046	1.584 ± 0.0158	0.3421 ± 0.0034	0.2637 ± 0.0026
	1550°C	1.27 ± 0.19	0.0240 ± 0.0005	0.0341 ± 0.0007	0.1074 ± 0.0016	0.9190 ± 0.0092	0.1590 ± 0.0024	0.8120 ± 0.0081	0.3713 ± 0.0037	0.3077 ± 0.0031
	Total	26.06 ± 3.9	0.0302 ± 0.0006	0.0484 ± 0.0010	0.1541 ± 0.0023	1.0237 ± 0.0102	0.1887 ± 0.0028	1.0820 ± 0.0108	0.3629 ± 0.0036	0.2989 ± 0.0030
B	550°C	3.88 ± 0.58	0.0130 ± 0.0003	0.0168 ± 0.0003	0.0888 ± 0.0013	1.0476 ± 0.0057	0.1608 ± 0.0024	0.8487 ± 0.0085	0.4158 ± 0.0041	0.3466 ± 0.0035
	950°C	9.12 ± 1.36	0.0139 ± 0.0003	0.0197 ± 0.0004	0.1184 ± 0.0018	1.0667 ± 0.0107	0.1679 ± 0.0025	0.9604 ± 0.0096	0.3368 ± 0.0034	0.2747 ± 0.0030
	1250°C	47.9 ± 7.2	0.0536 ± 0.0011	0.0896 ± 0.0018	0.1916 ± 0.0029	1.0286 ± 0.0103	0.2105 ± 0.0032	1.2027 ± 0.0120	0.3184 ± 0.0032	0.2527 ± 0.0025
	1550°C	5.1 ± 0.76	0.0707 ± 0014	0.1530 ± 0.0031	0.2617 ± 0.0039	1.1429 ± 0.0114	0.2535 ± 0.0038	1.5099 ± 0.0151	0.2982 ± 0.0030	0.2380 ± 0.0024
	Total	66.03 ± 9.9	0.0471 ± 0.0009	0.0806 ± 0.0016	0.1809 ± 0.0027	1.0438 ± 0.0104	0.2050 ± 0.0031	1.1722 ± 0.0117	0.3251 ± 0.0032	0.2601 ± 0.0026
	Blanks	($\times 10^{-10}$ cc STP) 0.009 (550°C); 0.015 (950°C); 0.022 (1250°C); 0.035 (1550°C)								

Xenon data are normalized to $^{132}Xe \equiv 1.00$.

*A = 40–90 μ; B = 90–200 μ.

Table 3. Concentration and isotopic composition of neon and argon in size fractions of 10084 soil.

Size fraction*	Temperature fraction	^{22}Ne (10^{-8} cc STP/g)	^{36}Ar	$^{20}Ne/^{22}Ne$	$^{21}Ne/^{22}Ne$	$^{38}Ar/^{36}Ar$	$^{40}Ar/^{36}Ar$
A	550°C	264.0 ± 27.0	272.0 ± 27.0	12.50 ± 0.13	0.0253 ± 0.0010	0.2470 ± 0.0031	3.469 ± 0.037
	950°C	1614.0 ± 161.0	823.0 ± 82.0	12.33 ± 0.12	0.0513 ± 0.0010	0.2441 ± 0.0027	2.303 ± 0.002
	1250°C	1245.0 ± 124.0	1104.0 ± 110.0	11.98 ± 0.12	0.078 ± 0.0016	0.2983 ± 0.0031	2.384 ± 0.024
	1550°C	140.0 ± 14.0	273.0 ± 27.0	12.23 ± 0.12	0.1013 ± 0.0020	0.3403 ± 0.0035	6.850 ± 0.069
	Total	3263.0 ± 326.0	2472.0 ± 247.0	12.21 ± 0.12	0.0615 ± 0.0012	0.2793 ± 0.0028	2.970 ± 0.030
B	550°C	288.0 ± 29.0	469.0 ± 47.0	12.51 ± 0.13	0.0328 ± 0.0010	0.1694 ± 0.0017	3.643 ± 0.038
	1250°C	281.0 ± 28.0	6734.0 ± 673.0	13.03 ± 0.13	0.0426 ± 0.0010	0.5133 ± 0.0056	2.086 ± 0.022
	1550°C	813.0 ± 81.0	127.0 ± 13.0	12.76 ± 0.13	0.062 ± 0.0012	0.2807 ± 0.0029	10.45 ± 0.104
	Total	1382.0 ± 138.0	7330.0 ± 733.0	12.33 ± 0.12	0.052 ± 0.001	0.4872 ± 0.0049	2.331 ± 0.023
C	550°C	2825.0 ± 282.0	1605.0 ± 160.0	12.63 ± 0.13	0.0397 ± 0.0010	0.1593 ± 0.0016	3.889 ± 0.040
	950°C	3002.0 ± 300.0	7175.0 ± 717.0	12.47 ± 0.12	0.0444 ± 0.001	0.2466 ± 0.0025	1.336 ± 0.014
	1250°C	1103.0 ± 110.0	7373.0 ± 737.0	11.86 ± 0.12	0.052 ± 0.0016	0.2590 ± 0.0028	1.458 ± 0.015
	1550°C	34.0 ± 3.4	809.0 ± 81.0	10.40 ± 0.11	0.151 ± 0.0030	0.2638 ± 0.0030	3.172 ± 0.032
	Total	6964.0 ± 696.0	16962.0 ± 1696.0	12.43 ± 0.13	0.044 ± 0.001	0.2446 ± 0.0024	1.718 ± 0.172
	Blanks	($\times 10^{-8}$ cc STP) ^{22}Ne: 0.018 (550°C); 0.014 (950°C); 0.036 (1250°C); 0.108 (1550°C) ^{36}Ar: 0.004 (550°C); 0.01 (950°C); 0.02 (1250°C); 0.04 (1550°C)					

*A = 40–90 μ; B = 90–200 μ; C = 200–1000 μ.

The radiogenic ^{40}Ar in 40–90, 90–200, and 200–1000 μ size fraction is 0.72×10^{-4}, 1.7×10^{-4}, and 2.91×10^{-4} cc STP/g, respectively. If we take K-contents of 1135, 1250, and 1580 ppm for these respective size fractions of 10084 from Basford *et al.* (1974), then the K–Ar ages for these sizes turn out to be 4.3, 5.56, and 6.11 b.y., respectively.

Component tracers

^{126}Xe is produced mainly by high energy galactic cosmic ray spallation whereas ^{132}Xe is produced by both GCR and SCR spallation reactions with barium isotopes. Additionally ^{132}Xe is shielded from any contribution from

Table 4. Isotopic composition of xenon in different size fractions of etched 10084 soil.

Size fraction*	Temperature fraction	(^{132}Xe) (10^{-10} cc STP/g)	124	126	128	129	130	131	134	136
A	550°C	2.25 ± 0.34	—	0.0517 ± 0.0013	0.1829 ± 0.0027	0.9861 ± 0.0099	0.1981 ± 0.0030	0.8135 ± 0.0081	0.5364 ± 0.0054	0.4543 ± 0.0045
	950°C	3.86 ± 0.58	—	0.0293 ± 0.0007	0.0910 ± 0.0014	1.0020 ± 0.0100	0.1321 ± 0.0020	0.8213 ± 0.0082	0.3698 ± 0.0039	0.2391 ± 0.0025
	1250°C	11.57 ± 1.74	0.0160 ±0.0004	0.0472 ± 0.0009	0.1445 ± 0.0025	1.1046 ± 0.0115	0.1528 ± 0.0025	0.9565 ± 0.0098	0.3559 ± 0.0037	0.3225 ± 0.0034
	1550°C	8.20 ± 1.23	0.146 ± 0.0003	0.0357 ± 0.0008	0.1036 ± 0.0016	1.0352 ± 0.0106	0.1745 ± 0.0028	0.9304 ± 0.0095	0.3646 ± 0.0038	0.2707 ± 0.0029
	Total	25.88 ± 3.88	0.0154 ± 0.0004	0.0413 ± 0.0010	0.1269 ± 0.0020	1.0570 ± 0.0106	0.1605 ± 0.0030	0.9156 ± 0.0092	0.3764 ± 0.0038	0.3051 ± 0.0030
B	550°C	1.59 ± 0.24	0.0383 ± 0.0010	0.0217 ± 0.0006	0.0631 ± 0.0010	1.0898 ± 0.0110	0.1292 ± 0.0020	0.8464 ± 0.0086	0.2885 ± 0.0030	0.2228 ± 0.0025
	1250°C	51.25 ± 7.69	0.0219 ± 0.0005	0.0296 ± 0.0007	0.1213 ± 0.0019	1.0370 ± 0.0105	0.2049 ± 0.0034	0.8884 ± 0.0090	0.3344 ± 0.0035	0.2889 ± 0.0030
	1550°C	7.69 ± 1.19	0.0175 ± 0.0005	0.0295 ± 0.0006	0.0744 ± 0.0011	1.0157 ± 0.0105	0.1736 ± 0.0028	0.8519 ± 0.0087	0.5208 ± 0.0057	0.3913 ± 0.0040
	Total	60.8 ± 9.12	0.0218 ±0.0005	0.0294 ±0.0007	0.1136 ± 0.002	1.0356 ±0.0104	0.1988 ±0.0036	0.8825 ±0.0088	0.3576 ±0.0036	0.3006 ±0.0030
	Blanks	($\times 10^{-10}$ cc STP) 0.004 (550°C); 0.005 (950°C); 0.009 (1250°C); 0.015 (1550°C).								

Xenon data are normalized to $^{132}Xe \equiv 1.00$.

*A = 40–90 μ; B = 90–200 μ.

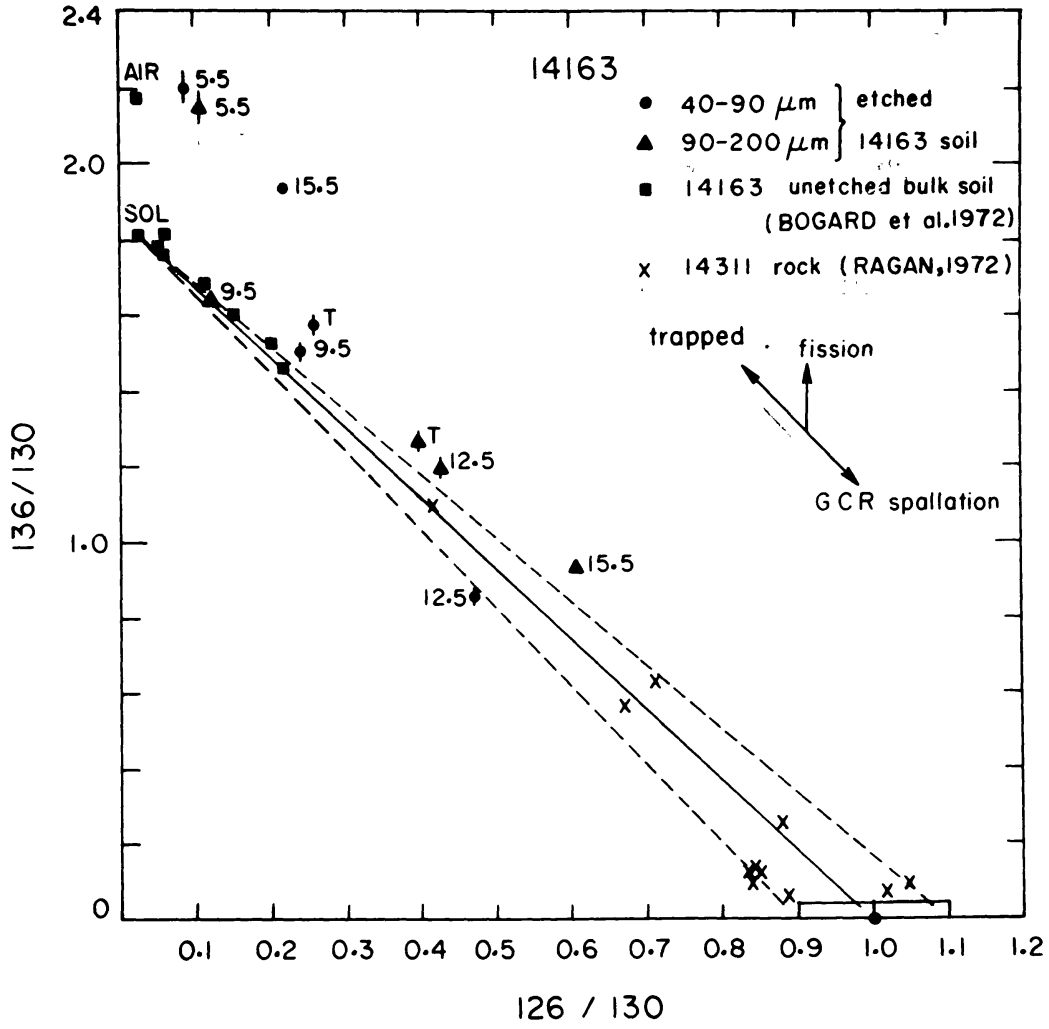

Fig. 2. Three isotope xenon diagram for computing fission correction. It is assumed that $(136/130)_{sp}$ is equal to zero. Deviations from the mixing line in the direction of excess ^{136}Xe are used to calculate the quantity of $(^{136}Xe)_f$. Other explanations are similar to those given for Fig. 4.

neutron poor isotopes produced in spallation of REE. ^{129}Xe and ^{131}Xe isotopes also have GCR and SCR contributions.

^{132}Xe isotope may have a sizable amount of fission. In order to calculate the fission contribution, it is assumed that spallation ^{136}Xe is negligible. This allows ^{136}Xe to be a typical indicator for fission xenon. If a temperature fraction has a fission component, the datum point moves vertically up as shown in Fig. 2 and the deviation of the point from the "mixing" line is proportional to $(^{136}Xe)_f$ present in that fraction. In order to calculate the $(^{132}Xe)_f$, it is assumed that $(^{132}Xe/^{136}Xe)_f$ has a value 0.67 in between the ^{244}Pu and ^{235}U (spontaneous and neutron induced) fission ratios because it is not clear which element is the main source of fission xenon in this case. The ^{132}Xe excesses, after corrections for trapped, fission, and GCR spallation components are attributed to SCR production in lunar fines.

In the case of ^{131}Xe there is a neutron-capture produced component on ^{130}Ba. The problem of estimating the neutron-capture component in Apollo 14 samples is discussed by Marti *et al.* (1973). They find that the $(^{131}Xe/^{126}Xe)_{sp} = 3.0–3.2$ for several lunar soils and rocks and the $(^{131}Xe)_n/(^{126}Xe)_{sp} = 2.0–2.2$. As a first-order approximation, the $(^{131}Xe)_{sp+n}/(^{126}Xe)_{sp}$ could be considered to be about 5.7 in these samples. By assuming that $(^{131}Xe)_f$ is small, the $^{126,130,131}Xe$ system could be described in three isotopes diagram where one end member is BEOC-12 and the other end member is represented by the combined GCR + (n, γ) components. The resulting deviations of the experimental points from this mixing line are attributed to SCR-produced ^{131}Xe in lunar soils. This represents maximum correction from GCR spallation and neutron-capture effects and the residual ^{131}Xe is therefore a lower limit of SCR contribution.

$^{130}Xe/^{128}Xe$ vs $^{126}Xe/^{128}Xe$ plots were also constructed to find out the behaviour of the experimental data. In fact, these plots are used to calculate SCR–^{130}Xe.

Discussion

Track irradiation records

The track irradiation characteristics of the lunar soils can be conveniently represented by two parameters (Arrhenius *et al.*, 1971): the quartile track density ρ_q, and the fraction of track rich grains, N_H/N. The value ρ_q, below which 25% of the grains in a given sample have their track densities, is essentially a measure of the integrated surface exposure duration of a lunar soil. The value of N_H/N, where N_H is the number of crystals having a track gradient or high track density ($\geqslant 10^8$ cm^{-2}), out of a total of N crystals analysed in a sample, is a good measure of the fraction of grains in a soil that has received solar flare heavy nuclei iradiation within the top few millimeters of the lunar regolith.

We show in Table 5 the values of these parameters in the two grain size fractions for the sample 10084 and 14163. It can be easily seen that both the ρ_q and N_H/N values for the sample 10084 are higher than that in the case of 14163 indicating a longer near surface exposure duration and a higher level of solar flare irradiation dose for 10084. Further the values are nearly the same, in each case, for both the A and B size fractions. The N_H/N value of 0.9 in the case of

Table 5. Fossil track data for lunar soil 10084 and 14163.

Sample	Size fraction*	No. of crystals analysed (N)	N_H/N	ρ_q ($\times 10^6$ cm^{-2})
10084	A	20	0.9	100
	B	60	0.92	100
14163	A	30	0.5	26
	B	60	0.47	32

*A = 40–90 μ; B = 90–200 μ.

10084 implies that at least 90% of the grains in this sample have received solar flare irradiation, whereas the corresponding value in the case of 14163 is ≈50%.

Noble gas elemental abundances

The elemental abundances of ^{22}Ne, ^{36}Ar, and ^{132}Xe in the unetched soils 10084 and 14163 (Bogard and Nyquist, 1972; Hintenberger *et al.*, 1970) for several size fractions are given in Table 6, along with the abundances measured in this study. A comparison of the data indicates that about 90% of the solar wind is removed from 14163-A and 10084-A (65% based on ^{22}Ne) whereas about 50–60% of solar wind is removed in case of 14163-B and 10084-B by our etching techniques. The incomplete removal of solar wind during etching can be attributed to inefficient etching of ilmenites and residual solar wind ions trapped in the glassy agglutinates.

Table 6. Effectiveness of etching in different size fractions of 14163 and 10084.

Sample	Size fraction*	Isotope	Noble gas content (cc STP/g) Unetched soil (a, b)	Noble gas content (cc STP/g) Etched soil	Solar wind removed (%)
14163	A	^{22}Ne	37.6×10^{-6}	4.68×10^{-6}	88.0
	B	^{22}Ne	22.7×10^{-6}	12.03×10^{-6}	48.0
	A	^{36}Ar	164×10^{-6}	6.4×10^{-6}	96.0
	B	^{36}Ar	94×10^{-6}	42.38×10^{-6}	55.0
	A	^{132}Xe	33×10^{-9}	2.6×10^{-9}	92.0
	B	^{132}Xe	15×10^{-9}	6.6×10^{-9}	56.0
10084	A	^{22}Ne	94.4×10^{-6}	32.62×10^{-6}	65.0
	B	^{22}Ne	47.4×10^{-6}	13.82×10^{-6}	71.0
	A	^{36}Ar	2.36×10^{-4}	0.247×10^{-4}	90.0
	B	^{36}Ar	1.63×10^{-4}	0.7330×10^{-4}	55.0
	A	^{132}Xe	1.82×10^{-8}	0.259×10^{-8}	84.0
	B	^{132}Xe	1.59×10^{-8}	0.608×10^{-8}	62.0

(a) Bogard and Nyquist (1972); (b) Hintenberger *et al.* (1970).

Gas contents for unetched soils are taken from those size fractions, close to those mentioned here for etched ones.

*A = 40–90 μ; B = 90–200 μ.

ISOTOPIC ABUNDANCES

Neon

The stepwise heating data for the etched 10084 and 14163 size fractions are plotted in the three isotope diagram (Fig. 3). Most of the points (except 1550°C fraction) for the etched 14163-A and 14163-B do not fall on the "mixing" line joining solar wind to GCR spallation. Instead, the points define a separate line

within experimental errors. Also the 550°C and 950°C fractions of 10084-A and the 550°C fraction of 10084-B plot on this separate line. Only the 1250°C and 1550°C fractions of 10084-B and the 1550°C fraction of 10084-A fall on the GCR-mixing line. Frick *et al.* (1975) have measured 20/22 and 21/22 values in different grain size fractions of feldspar separates from 15421 soil and observed that the data do not fall on the "mixing line" of solar wind with GCR spallation. However, they define a separate line indicating the presence of solar proton-produced neon component, with a composition of $21/22 \approx 0.7$ and $20/22 \approx 2$. This is similar to the SCR-produced neon component ($21/22 \approx 0.4$ and $20/22 \approx 3.0$), determined by Walton *et al.* (1974) for soil 67701. Figure 3 shows a comparison of the data of Frick *et al.* (1975) with ours. Within experimental errors, the SCR-mixing line for 10084 and 14163 conforms to feldspar points of 15421. The

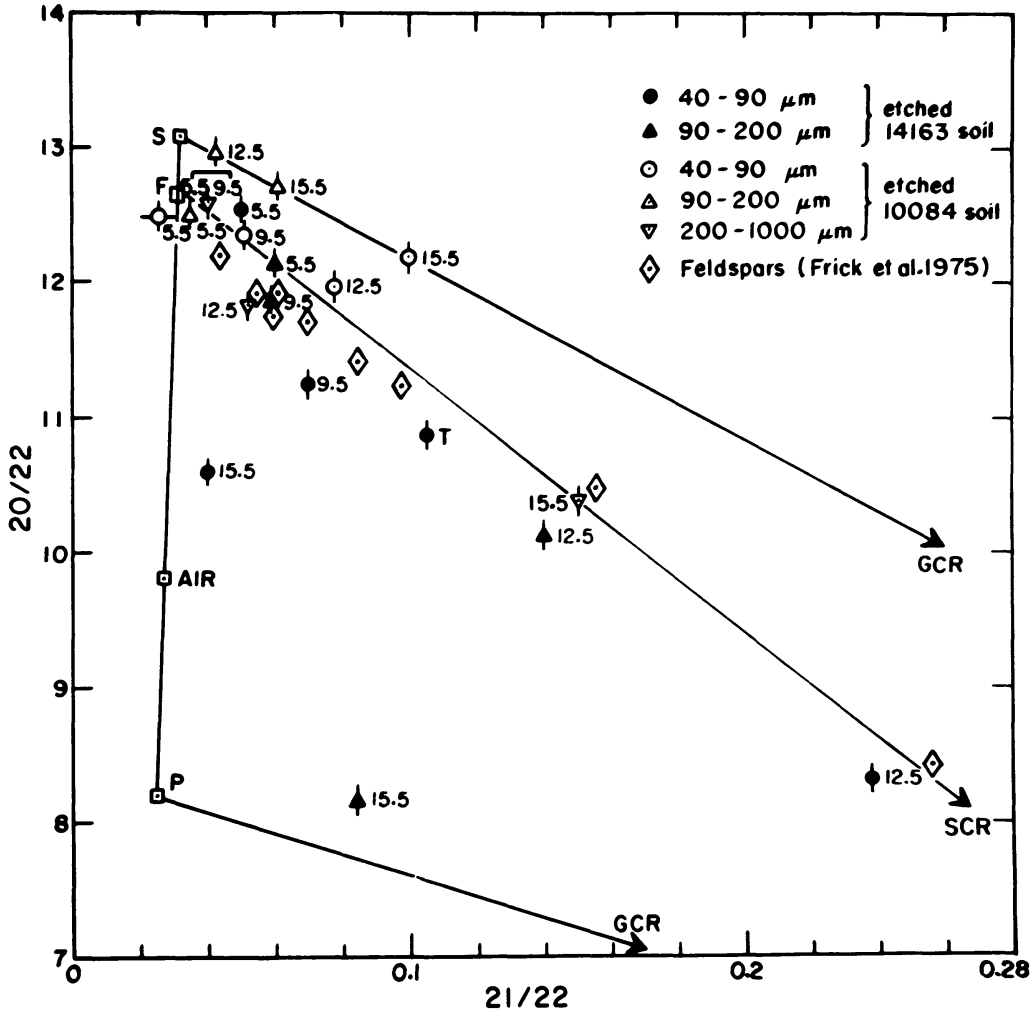

Fig. 3. Neon three isotope correlation diagram. S and P represent solar wind and planetary neon compositions while F represents the neon composition as deduced from the feldspar data of 15421 by Frick *et al.* (1975). The arrows labelled GCR and SCR join S to the two neon compositions: $20/22 = 0.9$; $21/22 = 0.87$ for GCR and $20/22 = 3.0$; $21/22 = 0.5$ for SCR, respectively. Our data seem to conform to line II of Walton *et al.* (1974).

scatter between the two sets of data may be due to minor differences in target chemistry or shielding conditions. The soils 10084 and 14163 provide definitive evidence for the presence of solar proton-produced neon component in lunar soils with a 21/22 ratio of ~0.5.

The SCR-21 excesses in the etched 10084 and 14163 soils are estimated using only those temperature fractions falling on the solar wind and SCR spallation "mixing" line. In these excesses, there may be some unknown contribution due to GCR and therefore these concentrations should be considered as upper limits

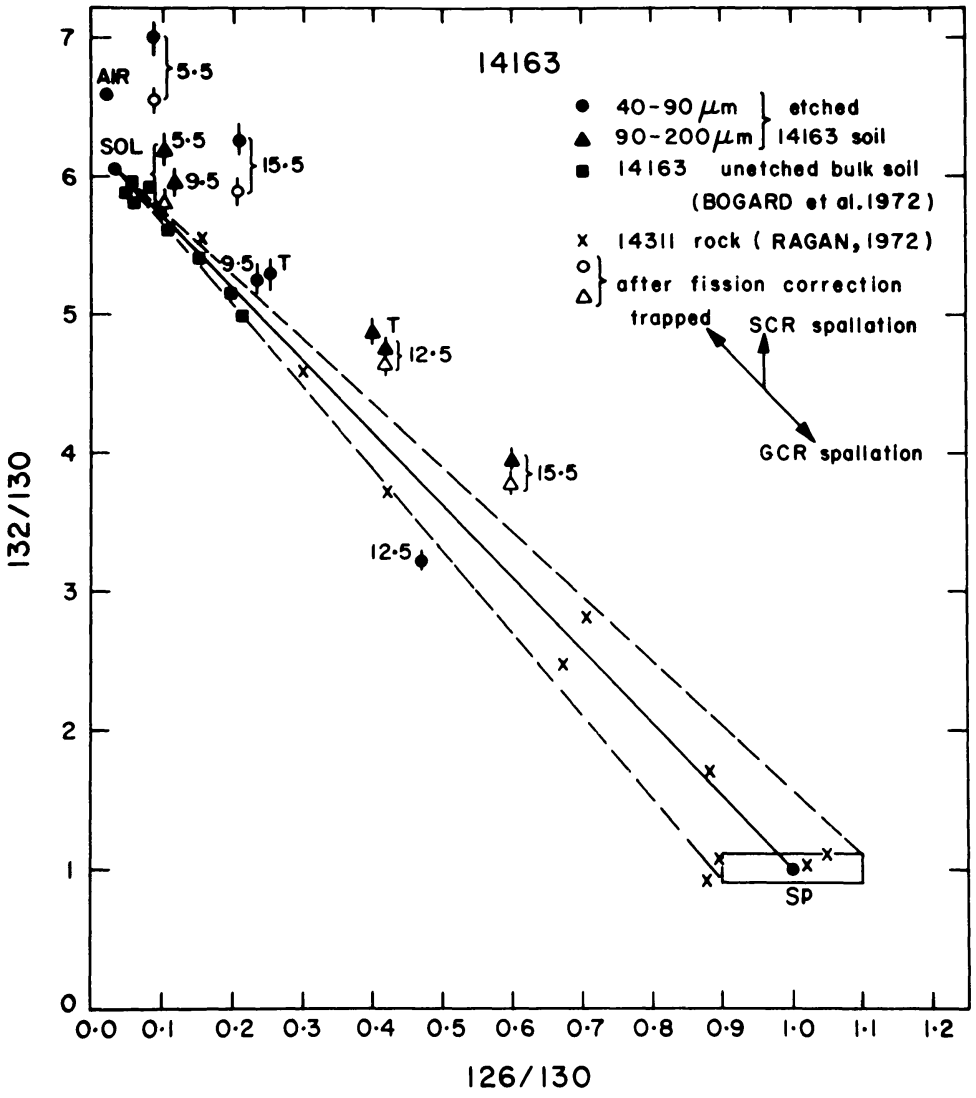

Fig. 4. Xenon three isotope correlation diagram for etched size fractions of 14163. The choice of the trapped and spallation components is discussed in the text. The stepwise heating data for 14311 rock (Ragan, 1972) is assumed to be typical for Apollo 14 rocks. Numerals close to the data points are release temperatures in hundreds of degrees centigrade. The isotopic ratios of 132/130 after fission correction are indicated by open symbols. Deviations from the line in the direction of ^{132}Xe are used to compute the concentration of ^{132}Xe due to SCR production.

of SCR contribution. In the case of 10084 and 14163, the weighted-mean SCR-21 excesses are calculated to be 103×10^{-8}cc STP/g and 53.1×10^{-8}cc STP/g, respectively.

Xenon

A-fraction. The 550°C temperature fraction for 10084-A (Fig. 5) yields 132/130 = 5.05, indicating negligible 132 excess due to SCR production. But the 550°C temperature fraction of 14163 (Fig. 4), yields a high 132/130 ratio of 7.0 after fission correction, indicating the presence of significant 132 excess due to SCR spallation. The 132 excess is observed to be 165×10^{-12}cc STP/g after applying the correction due to GCR spallation. The 132 release pattern for 14163 at 1250°C is opposite to that found in 550°C fraction. In case of 10084 the SCR-produced 132 is about 265×10^{-12}cc STP/g at 1250°C while in the case of 14163 at the same temperature, it is negligible. In the 950°C and 1550°C fractions approximately one fourth of the amounts of SCR-132 are seen in 10084 compared to 14163. The SCR-produced 132 excess in 10084-A is about 2.3 times that of 14163-A. This is in agreement with the track data which indicate that the

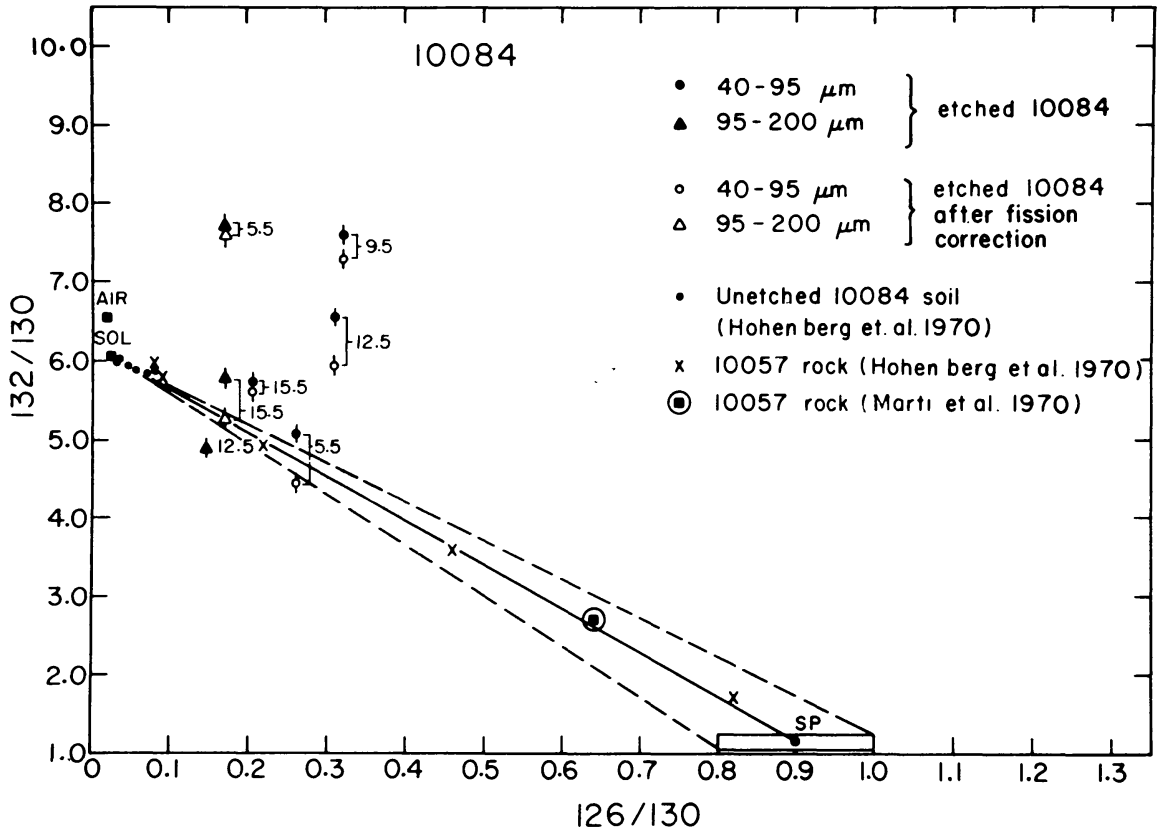

Fig. 5. Xenon three isotope diagram for etched size fractions of 10084. The stepwise heating data for 10057 (Hohenberg *et al.*, 1970) are assumed to be typical for Apollo 11 rocks. Other explanations are similar to those given in Fig. 4.

number of grains receiving solar flare irradiation is twice as much in 10084 compared to 14163 in this size fraction.

B-fraction. In this size fraction of 10084 about 25–30% of the total SCR-132 is released at 550°C and the 132/130 value is about 7.6 after fission correction. It should be noted that in 10084-B the 950°C release step was skipped and a single extraction was made at 1250°C. Even though the largest amount of total ^{132}Xe was released in this step no clear excess of SCR-132 could be detected after correction. But the situation for 14163 is different. Only about 2% of total SCR-132 is released in the 550°C fraction whereas about 80% is released in the 1250°C fraction. The total SCR-132 in this sample is about 1200×10^{-12} cc STP/g whereas it is only 400×10^{-12} cc STP/g for 10084.

Now we discuss briefly 129 release patterns in various size and temperature fractions of 10084 and 14163 (Figs. 6 and 7). In the 550°C fraction of 10084-A, SCR-129 excess is negligible, compared to about 110×10^{-12} cc STP/g estimated in the 14163-A. But at 1250°C, 14163-A shows negligible amounts whereas 10084-A has about 390×10^{-12} cc STP/g of SCR-129. The total 129 excess due to SCR production in 10084-A is about 4–5 times that in 14163-A. In many respects, the behaviour of SCR-produced 129 is similar to that of 132 in 10084 and 14163 size fractions at different temperatures.

The estimation of SCR-produced 131 is difficult because there is no direct way of finding $(131)_n$ due to (n, γ) capture on ^{130}Ba and also $(131)_{sp}$ yields are not correctly known. As mentioned earlier, in Fig. 8, $131_{sp} + 131_n$ is treated as a single component using a value of (131/126) = 5.7 (Marti *et al.*, 1973) for a soil fragment 14160,10. The 131 excesses, resulting after subtraction of trapped, GCR + (n,γ) components from total $(131)_n$ are attributed to SCR spallation. The total SCR-produced 131 in 10084-A is about 180×10^{-12} cc STP/g while it is 190×10^{-12} cc STP/g for 14163-A. The 10084-B yields a value of 250×10^{-12} cc STP/g for the total SCR-131 excess while for 14163-B, it is about 860×10^{-12} cc STP/g. As we do not know the relative contributions due to GCR spallation and neutron capture, larger uncertainties may be associated with the final SCR-131 excesses given here.

Comparison of GCR and SCR contributions in xenon

Varying amounts of GCR and SCR spallation components are observed in different temperature fractions of etched 10084 and 14163 size separates. In case of 14163-A the total GCR-126 released is about 120×10^{-12} cc STP/g while total SCR-132 is about 200×10^{-12} cc STP/g. At 550°C, very little GCR-126 and about 80% of SCR-132 are released; at 950°C roughly equal amounts of GCR and SCR components and at 1250°C and 1550°C more of GCR and little of SCR components are released. In the case of 10084-A, the total GCR-126 observed is $\sim 100 \times 10^{-12}$ cc STP/g while SCR-132 is $\sim 450 \times 10^{-12}$ cc STP/g. 50% of GCR-126 is released in 950°C and 1250°C fractions while 75% of SCR-132 is released in these temperature fractions. In 14163-B, about 70% of total GCR-126 and SCR-132 are released at 1250°C and the total SCR-132 observed in this sample is

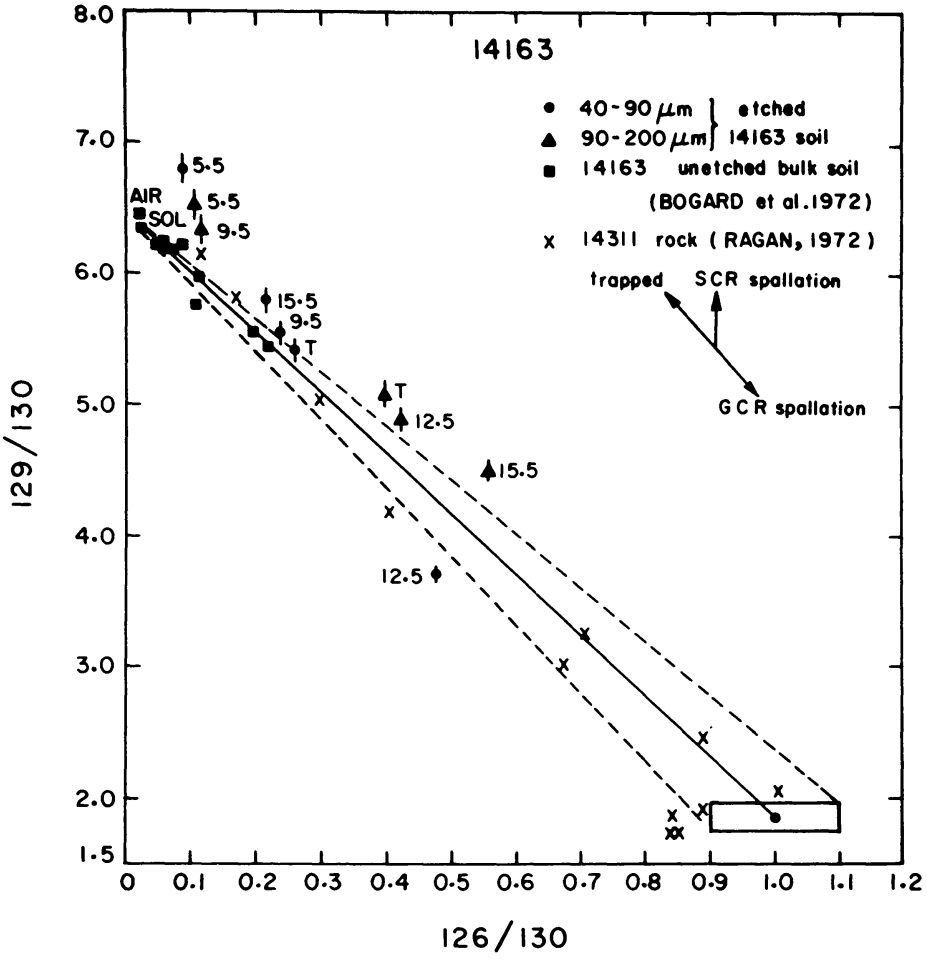

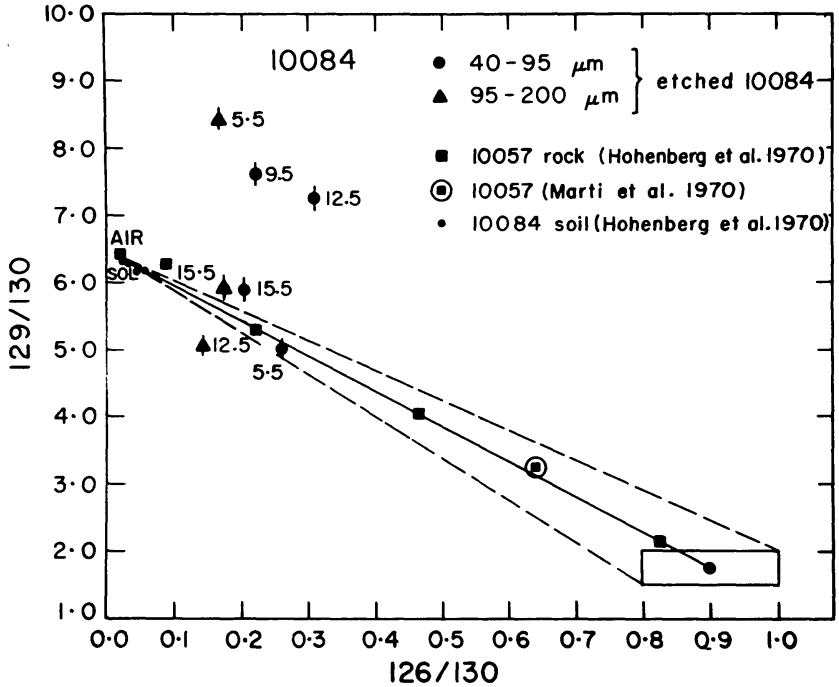

Figs. 6 and 7. Three isotope diagram for computing ^{129}Xe excess due to SCR production. This diagram in particular shows that SCR-129 excesses exist irrespective of the fact whether trapped gas is represented by solar or air composition. Note the similarity in the release patterns of 132 and 129 excesses in Figs. 4, 5 and Figs. 6, 7.

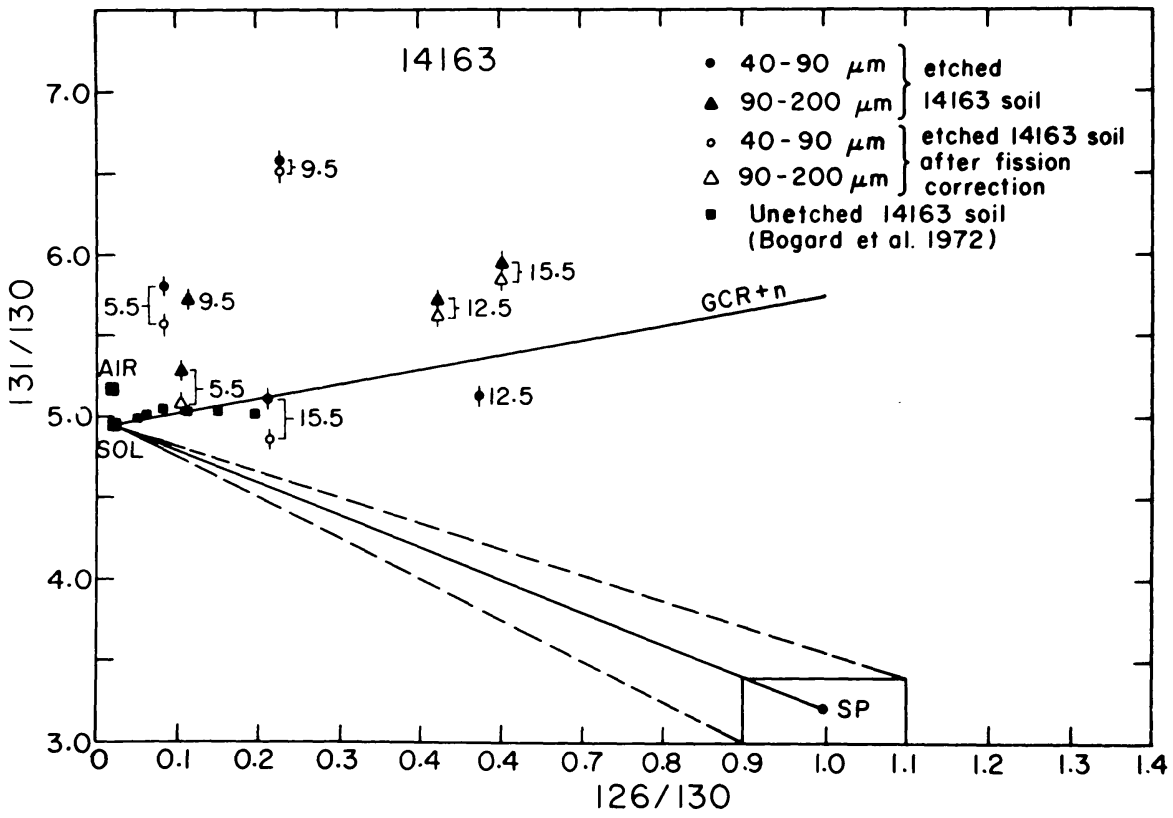

Fig. 8. Three isotope correlation diagram for calculating ^{131}Xe excess due to SCR production. The compositions of the end members in this diagram are discussed in the text. For comparison, we show pure GCR spallation as represented by "sp" (Marti *et al.*, 1973). Deviations from the "GCR + n" line in the direction of ^{131}Xe excess are used to find out the amount of SCR-131. A similar diagram results from the data from 10084 studies.

about 1.6 times that of GCR-126. Most of GCR-126 is released at 1250°C for 10084-B while no significant SCR-132 is released at this temperature. The dissimilar release patterns of GCR and SCR components at various temperature steps in these size fractions may relate to differences in mineralogy or target element contents or other reasons yet to be understood. We plan to work on mineral separates which may give additional insight into this problem.

SCR spallation xenon spectrum

The weighted-mean SCR-produced xenon excesses (normalised to 132) for both A and B fractions of 10084 and 14163 are given in Table 7 and in Fig. 9. These values are compared with low-energy xenon spallation spectra obtained by 38 and 50 MeV proton irradiation of barium targets by Kaiser *et al.* (1976) and Hussain (1976), respectively.

As pointed out above, the SCR-produced 131 calculated here could be considered as a lower limit because of maximum corrections applied for the GCR spallation plus neutron-capture component. It is likely that the SCR-produced 128 and 130 estimates may have larger uncertainties compared to SCR-129, 131,

Table 7. SCR-produced xenon isotope contents as obtained from 10084 and 14163 size fractions.*

Size fractions†	128	129	130	131	132	134
10084-A	0.08	1.01	0.07	0.44	1.00	0.09
14163-A	0.21	0.53	0.04	1.27	1.00	—
10084-B	—	1.30	0.31	0.60	1.00	0.10
14163-B	0.02	0.75	0.05	0.57	1.00	—

*These are the average values calculated from 128 and 130 normalisations.

†A = 40–90 μ; B = 90–200 μ.

and 132 isotopic excesses because the excess signals are relatively small in the former cases.

A general agreement between the spallation spectra, deduced from SCR-xenon excesses observed in 10084 and 14163 and those obtained from 38 and

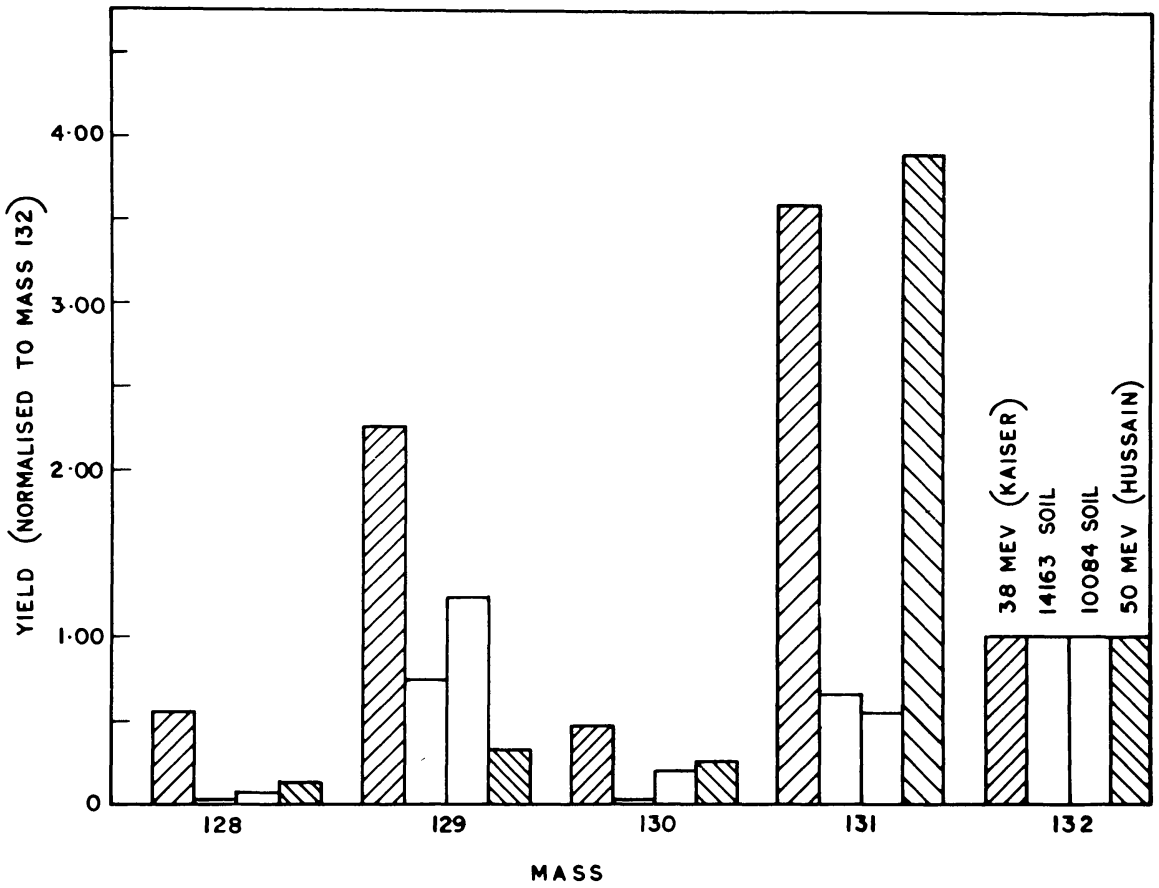

Fig. 9. Comparison of the spallation spectra as deduced from the SCR-produced xenon isotopic excesses (weighted-mean) observed in the etched size fractions of 10084 and 14163 with those obtained from 38 MeV (Kaiser *et al.*, 1976) and 50 MeV (Hussain, pers. comm., 1976) proton irradiation of Ba in laboratory experiments. The low yields for 131 are probably due to over-correction for GCR + neutron-capture component.

50 MeV proton irradiations of Ba seems to exist in the sense that the values for 10084 and 14163 fall between the limits set by 38 and 50 MeV proton irradiation of Ba. However, there are certain differences in detail. For example, the relative yields of 129 between 38 and 50 MeV are very different. It may be that the thresholds as well as the shape of excitation functions for different (p, α x p y n) and (p, x p y n) reactions change drastically in certain energy intervals in the low-energy region, leading to considerable variations in the production cross sections. In this energy region the excitation functions on Ba need to be determined. Also, the shielding effects may play an important role in the relative production of these xenon isotopes. In addition, part of the differences in the relative yields of SCR-produced 128-132 may be due to the following reason. ^{126}Xe, ^{129}Xe, and ^{131}Xe are produced by GCR spallation of both Ba and REE in varying amounts. But the shielded isotopes 130 and 132 are mainly produced by GCR spallation on Ba only. While applying GCR correction we have corrected for GCR-excesses based on total GCR-126 which may sometimes lead to an over-correction of GCR contribution for 130 and 132 isotopes whereas it makes only a minor change in the corrections due to 129 and 131.

"Solar flare" exposure ages of 10084 and 14163

We have noted earlier that it is possible to deduce the integrated surface exposure age of a lunar soil (layer) based on the observed track records in individual grains in the sample (Arrhenius *et al.*, 1971). However, it is not possible to deduce a meaningful "solar flare" exposure age of a layer because the total fluence of the solar flare particles received by a soil sample cannot be determined from the observed track data. Further, the extremely depth-sensitive track production rate coupled with complex motion of individual grains in the upper few millimeters of the lunar regolith (the "solar active" region) makes it difficult for an "average" track production rate to be used in deriving the solar flare exposure age. One can, however, consider the "surface" exposure age of a soil layer calculated on the basis of quartile track density (Arrhenius *et al.*, 1971) as an upper limit of its "solar flare" exposure duration. This is due to the fact that the track based "surface" exposure age gives the duration of exposure of the soil to both solar and galactic cosmic rays within a shielding depth of a few centimeters (the scooped depth of the sample). The isolation of the solar flare proton-produced noble gas components can lead to a better estimation of the "solar flare" exposure age of a soil layer, if the target chemistry, excitation function and the solar flare proton spectra are known. This is because one can deduce a reasonable "average production rate" in this case, since the depth dependence in the production rate in the first centimer of the regolith is not so sensitive as in the case of tracks. For example the production rate of solar flare produced Ne^{21} varies by only a factor of four in going from the surface of the lunar regolith to a depth of 5 mm.

Using solar flare proton spectra ($J_{E>10\,\mathrm{MeV}} = 100$ protons/cm^2 s 4π and $R_0 =$ 100 MV), according to Reedy and Arnold (1972) and Lal (1972) we calculate an average ^{132}Xe production rate of 2.3×10^{-14} cc STP per 10^{-6} g Ba per m.y. The

Table 8. "Solar flare" exposure ages determined by noble gas and fossil track methods.

Sample	Fossil track based surface exposure ages (m.y.)	Noble gas based "solar flare" exposure ages (m.y.)*	
		^{21}Ne	^{132}Xe
14163	~60	≤66	~43
10084	>100	≤130	~93

*See text for discussion on production rates.

^{132}Xe production cross section of 50 mb in the energy interval 20–65 MeV is derived from the reaction systematics in the krypton region from Sr and Zr (Sachdev *et al.*, 1969; Kantelo and Hogan, 1976) and the argon region from Ca (Walton *et al.*, 1974). In the case of neon, the 21 production rate is calculated to be 0.8×10^{-8}cc STP/g m.y. in the 0–5 mm depth region. This value is higher by a factor of 2.5 than that given by Reedy (1976). The ^{21}Ne exposure ages given in Table 8 are based on our calculated production rate.

Table 8 shows the "solar flare" exposure ages of the soil samples 14163 and 10084 as determined from the observed SCR-produced ^{21}Ne and ^{132}Xe concentrations and the fossil track based exposure ages. The agreement between the rare gas ages and track ages could be considered reasonable and the fact that the rare gas exposure ages are somewhat smaller than the track ages gives credence to the present method of estimation of solar flare exposure ages. The present work thus shows that this method can be used for estimating solar flare exposure ages of lunar soils (and rocks) in the time scale (>5 m.y.) in which the conventional methods using ^{26}Al and ^{53}Mn isotopes are ineffective due to saturation effects.

Note added in proof: The ^{21}Ne exposure ages in Table 8 is an underestimate since we use a production rate which is 2.5 times higher than that of Reedy (1976). If we take SCR (21/22) 0.3 (as a lower limit) instead of 0.5 that has been used in the text, it can account for a factor of 1.4 difference between exposure ages obtained by using Reedy's and our production values. Thus the solar flare exposure ages based on ^{21}Ne data seem to be inconsistent with those derived from xenon isotope and fossil track data. We may be in a better position to comment on these differences after the completion of our work on mineral separates of lunar samples which is underway.

Acknowledgments—We thank Prof. D. Lal for encouragement and valuable discussions regarding this work. We are greatly benefited from extensive discussions with Prof. K. Marti regarding this work. We are grateful to NASA for making these precious lunar samples available to us. The assistance rendered by Mr. J. R. Trivedi, Mr. M. M. Sarin, and Mr. S. K. Bhattacharya in some phases of this work is sincerely appreciated.

REFERENCES

Agrawal J. K., Gopalan K., and Rao M. N. (1974) Solar wind and cosmogenic rare gases in Lunar 16 and 20 soils and their correlation with cosmic-ray produced fossil tracks in lunar samples. *Pramana* **3**, 176–182.

Arrhenius G., Liang S., MacDougall D., Wilkening L., Bhandari N., Bhat S., Lal D., Rajagopalan G., Tamhane A. S., and Venkatavaradan V. S. (1971) The exposure history of Apollo 12 regolith. *Proc. Lunar Sci. Conf. 2nd*, p. 2583–2589.

Basford J. R. (1974) K–Ar analysis of Apollo 11 fines 10084. *Proc. Lunar Sci. Conf. 5th*, p. 1375–1388.

Bhandari N., Goswami J. N., Lal D., MacDougall D., and Tamhane A. S. (1972) A study of the vestigial records of cosmic rays using thick section technique. *Proc. Ind. Acad. Sci.* **LXXVIA**, 27–52.

Bogard D. D. and Nyquist L. E. (1972) Noble gas studies on regolith materials from Apollo 14 and 15. *Proc. Lunar Sci. Conf. 3rd*, p. 1797–1819.

Eberhardt P., Geiss J., and Grögler N. (1965) Über die Verteilung der Uredelgase im Meteoriten Khor Temki, *Mineral. Petrogr. Mitt.* **10**, 535–551.

Eberhardt P., Geiss J., Graf H., Grögler N., Mendia M. D., Mörgeli M., Schwaller H., Stettler A., Krähenbühl U., and Von Gunten H. R. (1972) Trapped solar wind noble gases in Apollo 12 Lunar fines 12001 and Apollo 11 brecia 10046. *Proc. Lunar Sci. Conf. 3rd*, p. 1821–1856.

Eberhard P., Geiss J., Graf H., Grögler H., Krähenbühl U., Schwaller H., and Stettler A. (1974) Noble gas investigations of lunar rock 10017 and 10071. *Geochim. Cosmochim. Acta* **38**, 97–120.

Frick U., Baur H., Ducati H., Funk H., Phinney D., and Signer P. (1975) On the origin of helium, neon, and argon isotopes in sieved mineral separates from an Apollo 15 soil. *Proc. Lunar Sci. Conf. 6th*, p. 2097–2129.

Gopalan K. and Rao M. N (1975) Enhanced solar cosmic ray flux in early solar system. Cosmic Ray Conference, 14th International, Munich, p. 1607–1612.

Gopalan K. and Rao M. N. (1976) Rare gases in Bansur, Udaipur and Madhipura chondrites *Meteoritics* **11**, 131–136.

Gopalan K., Rao M. N., and Agrawal J. K. (1973) High sensitivity mass spectrometer for noble gases. Tata Institute of Fundamental Research *Tech. Report.*

Hintenberger H., Weber H. W., Voshage H., Wänke H., Begemann F., and Wlotzka F. (1970) Concentration and isotopic abundances of the rare gases, hydrogen and nitrogen in Apollo 11 lunar matter. *Proc. Apollo 11 Lunar Sci. Conf.*, p. 1269–1282.

Hohenberg C. M., Davis P. K., Kaiser W. A., Lewis R. S., and Reynolds J. H. (1970) Trapped and cosmogenic rare gases from stepwise heating of Apollo 11 samples. *Proc. Apollo 11 Lunar Sci. Conf.*, p. 1283–1309.

Hoyt H. P., Jr., Walker R. M., and Zimmerman D. W. (1973) Solar flare proton spectrum averaged over the last 5×10^3 yr. *Proc. Lunar Sci. Conf. 4th*, p. 2489–2502.

Kaiser W. A., Rosner K. P., and Herr W. (1976) The excitation functions of Ba (p,xpyn)... ^{M}Xe (M = 124–136) in the energy range from 38 MeV–600 MeV; The use of "cosmogenic Xenon for estimating "burial" depths and "real" exposure ages. *Geochim. Cosmochim. Acta.* In press.

Kantelo M. V. and Hogan J. J. (1976) Charged-particle emission in reactions of ^{90}Zr with 10–86-MeV protons. *Phys. Rev. C.* **14**, 64–75.

Lal D. (1972) Hard rock cosmic ray archaeology. *Space Sci. Rev.* **14**, 3–102.

Lal D., Murali A. V., Rajan R. S., Tamhane A. S., Lorin J. C., and Pellas P. (1968) Techniques for proper revelation and viewing of etch tracks in meteoritic and terrestrial minerals. *Earth Planet. Sci. Lett.* **5**, 111–119.

Leich D. A., Niemeyer S., Rajan R. S., and Srinivasan B. (1975) Rare gases in etched 10084 ilmenite: A search for trapped solar-flare rare gases. *Proc. Lunar Sci. Conf. 6th*, p. 2085–2096.

Marti K., Lugmair G. W., and Urey H. C. (1970) Solar wind gases, cosmic-ray spallation products and the irradiation history of Apollo 11 samples. *Proc. Apollo 11 Lunar Sci. Conf.*, p. 1357–1367.

Marti K., Lightner B. D., and Osborn T. W. (1973) Krypton and xenon in some lunar samples and the age of North Ray Crater. *Proc. Lunar Sci. Conf. 4th*, p. 2037–2048.

Ragan D. (1972) Apollo 14 rare gases: Pu-244 xenon. Ph.D. thesis, Washington University, St. Louis, Missouri.

Rao M. N., Gopalan K., Venkatavaradan V. S., and Wilkening L. (1971) Solar flare effects in lunar xenon. *Nature Phys. Sci.* **233**, No. 41, 114–117.

Reedy R. C. and Arnold J. R. (1972) Interaction of solar and galactic cosmic ray particles with the moon. *J. Geophys. Res.* **77**, 537–555.

Sachdev D. R., Porile N. T., and Yaffe L. (1967) Reactions of ^{88}Sr with protons of energies 7–85 MeV, *Can. J. Chem.* **45**, 1149–1160.

Shedlvosky J. P., Honda M., Reedy R. C., Evans J. C., Jr., Lal D., Lindstrom R. M., Delany A. C., Arnold J. R., Loosli H. H., Fruchter J. S., and Finkel R. C. (1970) Pattern of bombardment-produced radionuclides in rocks 10017 and in lunar soil. *Proc. Apollo 11 Lunar Sci. Conf.*, 1503–1532.

Walton J. R., Heymann D., Jordan J. L., and Yaniv A. (1974) Evidence for solar cosmic ray proton-produced neon in fines 67701 from the rim of North Ray Crater. *Proc. Lunar Sci. Conf. 5th*, p. 2045–2060.